

The vibrational and dielectric properties of diamond with N impurities: First principles study

L.L. Rusevich^a, E.A. Kotomin^a, A.I. Popov^{a,*}, G. Aiello^b, T.A. Scherer^b, A. Lushchik^c

^a Institute of Solid State Physics, University of Latvia, 8 Kengaraga str., LV-1063 Riga, Latvia

^b Karlsruhe Institute of Technology, Hermann-von-Helmholtz-Platz 1, D-76344, Eggenstein-Leopoldshafen, Germany

^c Institute of Physics, University of Tartu, W. Ostwald Str. 1, 50411, Tartu, Estonia

ARTICLE INFO

Keywords:

Diamond crystal

Impurities

Electronic states

Vibrational properties

Optical properties

ABSTRACT

The atomic and electronic structures as well as elastic and dielectric properties (including first simulations of loss tangent, $\tan \delta$) of diamond with nitrogen impurities are calculated using the first principles LCAO method and the hybrid functional B3LYP. The effect of the single nitrogen substitutional atom (*C-center*) on the Raman and IR absorbance spectra is analyzed and compared with other calculations. It is shown that nitrogen defects do not affect $\tan \delta$ at far IR region used in diamond windows in fusion reactors for plasma heating and stabilization.

1. Introduction

Due to high melting point, hardness, chemical and radiation stability, wide band gap and optical transparency in a wide energy range, diamond along with gemstones, has numerous medical and technological applications [1–4]. In particular, diamond windows are used in fusion reactors for transmission of high power microwave energy (a few MW) for plasma heating and diagnostics [5–9]. This demands materials with low dielectric losses, which could be considerably affected by defects therein. High quality chemical vapor deposition (CVD) diamonds show very low loss tangent (e.g. down to several 10^{-6} at 170 GHz [5,7–9]). In recent years there has also been an increase in the number of papers discussing the properties and demonstrating corresponding applications of diamond-based nuclear detectors with a focus on CVD diamond detectors [10–19]. In particular, the detection of thermal and fast neutrons using CVD diamond detectors has been successfully reported [11]. Diamond CVD detectors for nuclear and dosimetry applications have been extensively discussed in [12,13]. It has been more than once confirmed that diamond radiation detectors operate successfully at temperatures from 150 °C to 500 °C [13–17]. We also note that several experiments are reported in the literature on the evaluation of the radiation resistance to neutrons of diamond detectors, although most of them were performed on polycrystalline diamonds [13,18,19].

Many different impurities were detected and characterized in diamond to date [20]. These defects can affect mechanical properties and electrical conductivity of crystals and, therefore, might be exploited for

a wide variety of specific applications and cutting-edge technologies but only nitrogen and boron can be present in diamond structure at noticeable concentrations. Even diamond classification system based solely on the presence or absence of nitrogen and boron impurities in the lattice and the ways of nitrogen arrangement (see, e.g. [21,22]). Nitrogen is the most common impurity in diamond with a concentration of several tenths %, as determined by elastic recoil detection analysis (ERDA) measurements. Diamonds containing detectable by IR absorption spectroscopy amount of nitrogen belong to type I, while nitrogen-free diamonds to type II. Further sub-classification of type I diamond depends on how nitrogen atoms are arranged in the diamond lattice. If nitrogen is as single, isolated one from another, atoms, replaced in the lattice carbon atoms — it is type Ib diamond. Such N impurities in diamond are called *single substitutional N* or *C-centers*. Nitrogen can form various aggregated structures in diamond. Diamond with aggregated N impurities is a diamond type Ia. The most common N configurations for type Ia diamond are *A-centers* (IaA diamond), which consist of two N substitutional atoms, adjacent to each other in the lattice, and *B-centers* (IaB diamond) involves four N atoms around a carbon vacancy. Many other possible arrangements of N atoms in diamond lattice are not included in the diamond type classification. Type II diamonds are also divided into two types — IIa and IIb. Type IIb diamond contains single isolated boron substitutional atoms, while diamond of type IIa does not contain measurable boron impurities. Synthetic diamonds are most commonly types Ib or IIa, while *A-* and *B-centers* are mainly in natural crystals.

* Corresponding author.

E-mail address: popov@latnet.lv (A.I. Popov).

In this paper, we study the effects of nitrogen impurities since nitrogen is widely used in CVD diamond growth. Several theoretical papers were published recently on defects in diamond, including vacancies [23–27] and nitrogen related defects [26–31] with the main focus on the atomic and electronic structure. However, very little attention was paid in theoretical studies of insulating materials to their dielectric properties especially loss tangent $\tan \delta$ (see, e.g. [32]), what is one of our primary interest in this paper. We pay also attention to the spin states of paramagnetic defects largely neglected in previous studies (with rare exceptions [23,31]). In addition, we consider the defect-induced Raman and IR spectra and compare them with previous calculations as well as discuss the elastic properties of defective diamond.

2. Computational details

First-principles (*ab initio*) computer simulations were performed to investigate type Ib diamond crystal (with isolated nitrogen substitutional atom). The structural, elastic, electronic, dielectric and vibrational properties of this system, as well as defect formation energy were examined within the linear combination of atomic orbitals approximation as implemented in CRYSTAL17 computer code [33]. Prior the main simulation of the defective diamond, we performed the preliminary computations of the lattice constant, band gap and the Raman peak position for pristine diamond using three different all-electron basis sets for carbon atom description and three commonly used hybrid DFT-HF exchange-correlation functionals. We compared our results with available experimental data and define an optimal set up, which we used later for the *C-center* simulation (see Supplementary section S1, Table S1).

The main computations were based on B3LYP global hybrid functional and all-electron basis sets of Gaussian type functions with exponents for d-shell for carbon and nitrogen atoms (C_6-21d1 and N_6-21d1). A periodic supercell (SC) approach has been applied to consider a nitrogen substitutional atom in diamond lattice. In this study, we have used cubic SC containing 64 carbon atoms before substitution one of them by nitrogen atom and nitrogen concentration was $\approx 1.56\%$ ($\approx 2.75 \cdot 10^{21} \text{ cm}^{-3}$). The five thresholds governing the truncation of the Coulomb and exchange infinite lattice series have been set to 8, 8, 8, 8, 16, and a regular Monkhorst-Pack mesh of points in reciprocal space with shrinking factor 12 and 6 has been used for bulk and supercell calculations, respectively. The Self-Consistent Field (SCF) convergence threshold for the energy was set to 10^{-10} Hartree for both geometry optimization and vibration frequency calculations.

Nitrogen and carbon atoms are not isovalent atoms and, therefore, when carbon atom in diamond is substituted by nitrogen atom, not all chemical bonds are closed, the system has one unpaired electron associated with the carbon atom and effective spin of system is $S_z = 1/2$. To investigate spin state of system we used the unrestricted (open shell) DFT calculations.

An important issue, related to the computation, is a symmetry of the crystal with point defects. Since a geometry optimization depends on the symmetry, the choice of symmetry may affect many important parameters of the system (the total energy, spin distribution, defect formation energy etc.). During simulation of diamond with *C-center*, the replacing one carbon atom by nitrogen atom forms the defect in SC. At that, the exact position of the defect may affect the symmetry of the defective system. Generally, the symmetry is lowered upon the creation of a defect. Moreover, appearance in the system of atoms with different spins can further lower the symmetry. However, if is replaced atom in SC, which does not have any equivalent by symmetry atoms in this SC, the symmetry of system keeps the same (or, may be, is lowered only due to appearance of atoms with different spins). In this study, we performed simulations for two systems with different symmetry. In one case we replaced carbon atom which does not have equivalent by symmetry atoms in SC and got defective system with maximal symmetry (for given SC). Taking into account appearing of unpaired spin in the system, this SC has 6 symmetry operations and corresponds to the trigonal crystal

system (space group SG 160, R3m). In another case, we replaced carbon atom which has maximal quantity (11) of equivalent by symmetry atoms in SC. Taking into account unpaired spin, we got the system with 1 symmetry operation (SG 1), i.e., computations were performed without any symmetry. In more detail, see Supplementary section S1.

We have performed a complete vibrational analysis of both pristine diamond and diamond with *C-center*, including the one-phonon Raman and IR spectra simulation, as well as calculations of dielectric functions and loss tangent. The total dielectric tensor $\epsilon(\nu)$ is the sum of the electronic (high-frequency) and the vibrational components. The electronic contribution has been calculated through the coupled perturbed Hartree-Fock/Kohn-Sham (CPHF/CPKS) scheme, adapted for periodic systems [34,35]. The calculation of the transverse optical (TO) vibrational frequencies and vibrational contribution to the dielectric tensor were performed at the Γ -point (the center of the first Brillouin zone) within the harmonic approximation. The integrated intensity I_n of IR vibrational mode ν_n is computed under the hypothesis of isotropic response (i.e., powder sample). We have calculated IR intensities through both Berry phase approach, which implies numerical differentiations, and CPHF approach, which is entirely analytical [33,36]. Both methods give close intensities, as it was in the study concerning strontium titanate and barium titanate [37]. The relative Raman intensities are computed by a fully analytical method, which is based on the self-consistent solution of first- and second-order CPHF/CPKS equations for the electronic response to external electric fields at the equilibrium geometry [38,39]. Finally, the calculated Raman intensities are normalized to the highest peak, arbitrarily set to 1000.

Besides intensity, the one-phonon Raman and IR absorbance spectra were simulated using TO vibrational modes. Both types of spectra are described by the convolution of intensity with Lorentzian resolution function:

$$A(\nu) = \sum_n \frac{I_n}{\pi} \frac{\gamma_n/2}{(\nu - \nu_n)^2 + \gamma_n^2/4} \quad (1)$$

where ν_n and I_n are the computed TO frequencies and Raman or IR intensities, respectively, for each mode n ; γ_n is the full width at half maximum (FWHM) of resolution function.

Computation of elastic tensor is implemented in CRYSTAL17 code as a fully automated procedure. We have calculated elastic constants for pristine and defective diamond and compared obtained results with existing experimental data for pristine diamond (see Supplementary section S2).

3. Results and discussion

3.1. The structural and electronic properties

Carbon atoms are bonded by sp^3 bonds in the diamond crystal, as a result, each carbon atom connects with four more carbon atoms. Our calculations reveal that interatomic distance in pristine diamond is 1.554 Å. Structure of *C-center* has been investigated by several *ab initio* computations [28,31,40], which demonstrate that a nitrogen atom bonded to three carbon neighbors. The result of our simulation of *C-center* in 64-atom SC is presented in the Fig. 1. This simulation confirms that *C-center* undergoes a trigonal distortion: the nitrogen atom and one of the carbon atoms (C1 in the Fig. 1) move away from each other, the distance N—C1 increase to 2.060 Å (+33 %). On the other hand, bond lengths of nitrogen atom with three other nearest carbon atoms (C4, C13, C27), on the contrary, are reduced to 1.479 Å (−5 %). The calculations reveal that the local perturbation of the lattice decays very rapidly and bond lengths between carbon atoms in the second shell (relatively nitrogen atom) is changed to ~ 0.01 Å ($\pm 0.6\%$) only (see Fig. 1, C4—C_(a) and C4—C_(b) bonds).

Fig. 1 demonstrates also charge and spin distribution in the vicinity of the *C-center*. The simulation reveals that the main part of unpaired

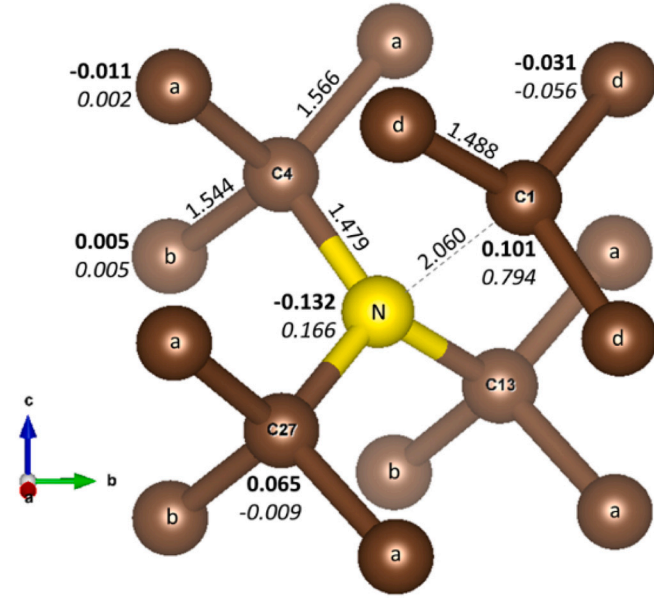


Fig. 1. The nearest vicinity of *C-center* (N substitutional atom in diamond) in 64-atom SC. Carbon atoms C4, C13 and C27 are equivalent by symmetry; a-, b-, d-noted carbon atoms are groups of atoms, equivalent by symmetry, too. Bond distance (in Å), Mulliken net charge and atomic spin (in $|e|$, **bold** and *italic*, respectively) are shown in the figure for each symmetry irreducible atom.

defect spin, 0.794 of electron spin (1 was as the initial guess), is localized on C1 carbon atom. It is the atom with unpaired electron, the most distant of the four nearest atoms to nitrogen, while the spin of nitrogen atom is only 0.166. This situation is an opposite to the substitution by nitrogen atom the oxygen atom in SrTiO₃. While the latter system also has one unpaired electron (and, hence, the spin of system is $S_z = 1/2$, too), the electron is associated with the nitrogen atom and main part of spin is localized on this atom [41]. Mulliken population analysis gives for charge of nitrogen atom $-0.132|e|$, for the nearest to nitrogen carbon atoms $+0.065|e|$, and for the carbon atoms of second shell $+0.005|e|$ and $-0.011|e|$, what means that these atoms are almost neutral. The charges of C1 and bonded with it C_(d) atoms are $+0.101|e|$ and $-0.031|e|$, respectively (Fig. 1).

Our results are in a reasonable agreement with data [31] obtained by the simulation of the *C-center* using of SC with 216 atoms. The significant differences are demonstrated only for the Mulliken charges of nitrogen atom ($-0.132|e|$ in our study vs. $-0.42|e|$ in [31]) and three carbon atoms, bonded with nitrogen ($+0.065|e|$ vs. $+0.13|e|$). Although, further analysis reveals that already the nearest vicinity of *C-center* provides almost complete neutrality of system in both cases. In particular, total charge of atoms represented in the Fig. 1 is $+0.020|e|$, but within the two shells relatively nitrogen atom $+0.012|e|$.

Note, that in Fig. 1 we show the results of simulation for a system with symmetry of SG 160 (we replaced in SC C33 carbon atom by nitrogen atom; see Figs. S1 and S2 in Supplementary). In this case atoms C4, C13 and C27 are equivalent by symmetry and there are another groups of equivalent by symmetry atoms in the SC (namely, groups of atoms C_(a), C_(b) and C_(d) in the Fig. 1). Interestingly, simulation of system with SG 1 (C34 carbon atom in SC is replaced by nitrogen atom; see Fig. S1 in Supplementary) gives surprisingly the same results that obviously confirms the correctness of the results of *C-center* simulation. Further, all presented data correspond to the computations with SG 160, unless another is said.

The calculated indirect band gap for pristine diamond, obtained in this study, is 5.7 eV, very close to the experimental value. A defect can modify the band gap. Note, in our simulations of systems with unpaired spins all electrons are divided into two groups: with spins up (alpha-

electrons) and with spins down (beta-electrons). The total spin of a system depends on the difference in the numbers of alpha- and beta-electrons. Our calculations of the electronic density of state (DOS, see Fig. 2) and the relevant band structure (see Supplementary Fig. S3) reveal that *C-center*, firstly, slightly decreases band gap value (to ≈ 5.5 eV) and, secondly, produces inside the band gap two local energy states (defect levels, or, to be exact, defect bands due to of interaction of periodically repeated defects). One of them is the occupied donor level, located ≈ 2 eV above the valence band (VB) top, with dispersion (width of band) ≈ 0.5 eV. The minimum energy difference between the bottom of the conduction band (CB) and the top of the in-gap donor defect band is ≈ 3.1 eV (indirect transition from defect band to CB for alpha-electrons). The second in-gap defect level is the unoccupied level (acceptor), which is located close to the CB bottom (≈ 0.1 eV below) and has dispersion ≈ 0.8 eV. The minimum energy difference between the bottom of the defect acceptor band and the top of the VB is ≈ 4.5 eV (direct transition for beta-electrons from VB to defect band). Based on this, we predict the optical absorption due to *C-center* around 3 eV.

Interestingly, our simulations reveal that both in-gap defect bands are mainly produced by the C1 carbon atom and only to a lesser extent by a nitrogen atom (see projected DOS in the Figs. S4, S5 in Supplementary), what coincides with conclusions [31].

We evaluated the *C-center* formation energy E_{form} by

$$E_{form} = E(N_{dop}) - E(N) + E(C) - E(pristine) \quad (2)$$

where $E(N_{dop})$ and $E(pristine)$ are the total energies of the crystal with and without nitrogen dopant, respectively, $E(N)$ is the half of the total energy of a gas-phase N₂ molecule and $E(C)$ is the energy of a single carbon atom in the pristine diamond [31]. The calculated formation energy is $E_{form} \approx 4$ eV, what is quite close to prediction in [31] (3.2–3.7 eV for SC with 64 atoms depending on the basis set).

3.2. IR and Raman spectra

In this study, we have performed a complete vibrational analysis of diamond with *C-center*, including calculation of TO phonon frequencies, intensities of the IR and Raman scattering and simulation of one-phonon IR and Raman spectra. For 64-atom SC there are 192 normal lattice vibrations at the Γ -point. Three of them are acoustic vibrations, the others optical ones, which are distributed over more than hundred nondegenerate (A) and double degenerate (E) modes. Some of these modes are silent modes (i.e., neither Raman-, nor IR-active), the others are both Raman- and IR-active. Most of active modes have very small, close to zero, intensities, and only a small part of them are presented by significant intensities. Note, that all calculated TO modes are located in the range of 495–1351 cm⁻¹ (14.8–40.5 THz).

As is known, defect-free diamond reveals no IR activity (not permitted by symmetry), but it appears due to defects. Thus, the calculated IR spectrum (the one phonon area) caused by N impurity (*C-center*) is presented in Fig. 3. As one can see, it is spread over the wide range, between 500 and 1350 cm⁻¹ (the largest 5 peaks are marked therein). Let us consider these five the most intensive peaks in more detail. Beside of the comparison of the displacements of atoms in the corresponding vibrational modes, for additional analysis of specific atoms contributions to the modes, we have used the isotopic substitution option (the possibility to change the atomic masses for individual atoms), which is implemented in the CRYSTAL code [33]. In particular, the influence of vibrations of N and C1 atoms as well as atomic cluster C4 + C13 + C27 (see Fig. 1) on the formation of some peaks in IR and Raman spectra was estimated. We have calculated isotopic shift of vibrational modes for three different cases: due to ¹⁴N \rightarrow ¹⁵N substitution, as well as ¹²C \rightarrow ¹³C substitution (for C1 atom and the mentioned cluster).

The analysis of atom displacements in A mode 713 cm⁻¹ reveals that N and C1 atoms show the maximal displacements. At the same time, the

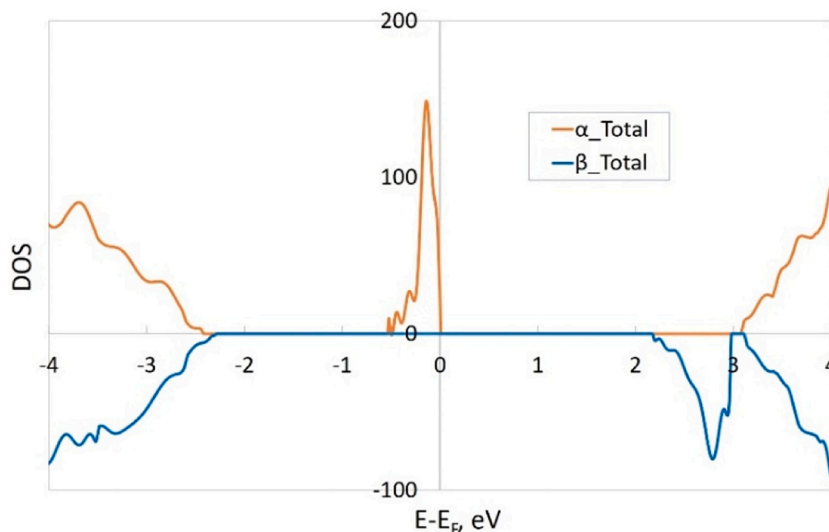


Fig. 2. The total electronic DOS for alpha- and beta-electrons in diamond with *C-center*. The zero energy value corresponds to the Fermi level.

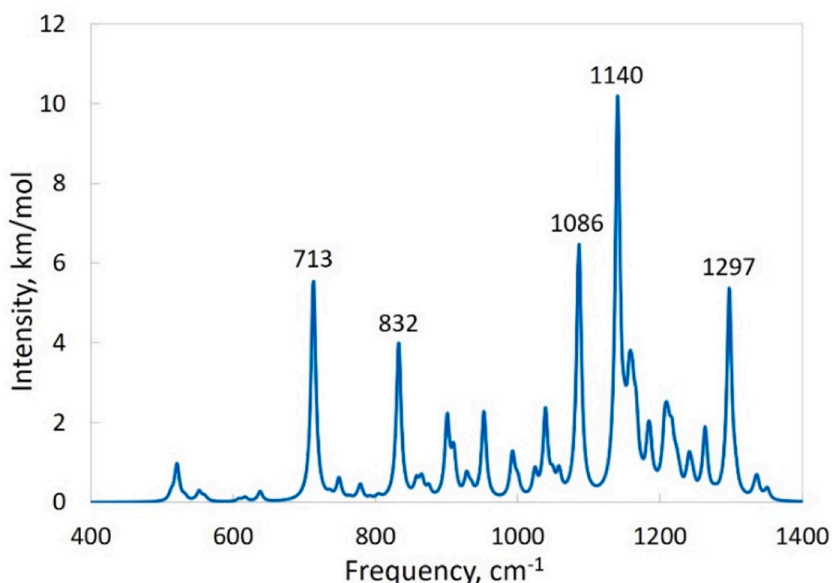


Fig. 3. The simulated IR absorbance spectrum of *C-center* in the diamond. Numbers in the figure show the frequencies of the peaks (in cm^{-1}).

isotopic shifts are 5.2 cm^{-1} and 5.8 cm^{-1} for N and C1 atoms, respectively. The situation with *A* mode 832 cm^{-1} is almost the same: N and C1 atoms show the maximal displacements, the isotopic shifts are 3.0 cm^{-1} (for N atom) and 3.4 cm^{-1} (C1 atom). N atom demonstrates the maximal displacement in *E* mode 1086 cm^{-1} , isotopic shift of line due to N atom is 2.3 cm^{-1} . The most intensive peak (1140 cm^{-1}) in the spectrum is connected with *E* vibrational mode. N atom and cluster of three the nearest to it carbon atoms give the largest vibrational contributions to this peak. The isotopic shifts are 5.3 cm^{-1} (for N atom) and 12.9 cm^{-1} (for the cluster of the three carbon atoms). Interestingly, both these isotopic shifts are the maximal shifts due to these atoms if to consider all vibrational modes. C1 atom gives the largest contribution to the formation of the fifth main peak (*E* mode 1297 cm^{-1}) in the IR spectrum. Isotopic shift of this line (10.4 cm^{-1}) is the largest among shifts of all lines due to C1 atom. Note here that this TO vibrational mode (1297 cm^{-1}) plays also essential role in formation of Raman spectrum (see below).

Finishing the consideration of the IR spectrum, we emphasize that all

observed peaks arise due to the perturbation of the crystal lattice by the defect and the vibrations of N atom and the closest to it carbon atoms make the substantial contribution to this spectrum. The comparison of our simulated spectrum with one [31] shows that these spectra are in very good agreement.

In contrast to the IR, defect-free diamond has one distinctive Raman peak at 1332 cm^{-1} [2,3] and our calculations perfectly reproduce this experimental value of Raman peak position (see Table S1 in Supplementary). The simulated first-order Raman spectrum for diamond with *C-center* is presented in the Fig. S6 in Supplementary. A feature of this spectrum is that its main peaks are located in a narrow area $1300\text{--}1350 \text{ cm}^{-1}$. Our simulations predict that there are two strong and one smaller peaks in the spectrum of defective diamond, which are located close to position of the peak for pristine diamond (Fig. 4).

As the density of the vibrational modes with essential intensities in a narrow range $1300\text{--}1350 \text{ cm}^{-1}$ is quite large, in this case there are no direct corresponding of the vibrational modes and the spectral peaks in the Raman spectrum of diamond with the *C-center*. The five most

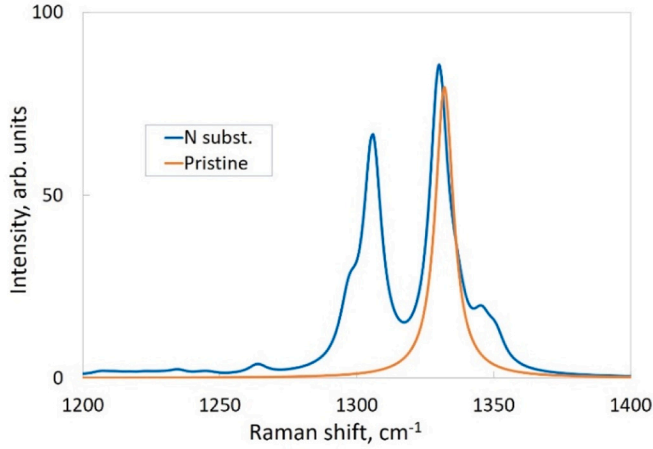


Fig. 4. Simulated Raman spectra for pristine diamond and diamond with nitrogen substitutional atom (with *C-center*). The relative intensities of two spectra are arbitrary. FWHM of resolution function, used in simulation, is 8 cm^{-1} .

intensive Raman lines are 1297 cm^{-1} (*E* mode; intensity 0.20), 1306 cm^{-1} (*A* mode; intensity 0.77), 1330 cm^{-1} (*E* mode; intensity 1.0), 1336 cm^{-1} (*E* mode; intensity 0.13) and 1346 cm^{-1} (*A* mode; intensity 0.12). Intensities of the Raman lines, which are presented in the parentheses, are normalized per the line with the largest intensity. Note that the first mentioned mode (the most low frequency mode, 1297 cm^{-1}) is the same, which we discussed as the most high frequency mode in the IR spectrum. It is clear that convolution with resolution function (even with $\text{FWHM} = 8 \text{ cm}^{-1}$) makes “blurred” system of peaks in the spectrum. The first peak in the spectrum (Fig. 4) is formed, mainly, by two first modes (1297 cm^{-1} and 1306 cm^{-1}), the most intensive peak (which position is very close to the position of peak in spectrum of pristine diamond) arises due to modes 1330 cm^{-1} and 1336 cm^{-1} , the main contribution to the third peak gives the mode 1346 cm^{-1} .

We already have determined above that C1 atom give the largest vibrational contributions to the mode 1297 cm^{-1} . It means that C1 atom is related with formation of first peak in the Raman spectra of defective diamond. Therefore, it is possible to consider this peak as “new” peak, which arises due to presence of *C-center* in diamond. Concurrently, no one of the four remaining the most intensive Raman lines has essential contribution of *C-center* and its nearest neighbors. For example, isotopic shift of the most intensive line (1330 cm^{-1}) is almost absent for N atom and is only 0.2 cm^{-1} for both C1 atom and the cluster. It means that vibrational contributions of the defect to the formation of second peak is negligible and the “mechanism” of formation of this peak is the same, as in the pristine diamond. Therefore, it is possible to consider the second peak as “old” peak, which was in the defect-free crystal. On the other hand, the line 1336 cm^{-1} demonstrates an isotopic shift 0.6, 0.3 and 3.8 cm^{-1} for N atom, C1 atom and the cluster, respectively. Perhaps, such defect contribution can explain the shift of second peak by a few cm^{-1} in comparison with peak position in the pristine diamond.

We suppose that the presence of two peaks in a narrow area is a specific characteristic of Raman spectra for diamond with *C-center*. This feature of spectrum can be used for identification of such type of defect. The distance between peaks is approximately 30 cm^{-1} . We have performed simulation of Raman spectrum with FWHM equal to 30 cm^{-1} , what is, evidently, closer to the experimental conditions. Fig. S7 in Supplementary demonstrates two Raman spectra with different FWHM — 8 and 30 cm^{-1} . Even with wider resolution function, two peaks in the spectrum remain distinct, what gives hope for the experimental use of the predicted spectrum feature.

At the end of this sub-section, we would comment on the vibrational properties of system with SG 1, when C34 carbon atom in SC is replaced

by nitrogen atom (see Supplementary section S1, Fig. S1). Note some differences in the vibrational spectrum. Firstly, degeneration of *E* modes is removed, and each of them is split into two nondegenerate *A* modes with very close frequencies (the splitting does not exceed a few tenths of cm^{-1}). At the same time, the intensity of the initial *E* mode is divided almost equally between the two new *A* modes. Secondly, the silent modes are absent; all modes in phonon spectrum are both IR- and Raman-active. On the other hand, these new active modes have zero or almost zero intensities. Thus, the mentioned differences in the phonon spectra will not affect the IR and Raman spectra, which are simulated with a finite width of the resolution function.

3.3. Dielectric properties

To characterize dielectric losses in material, the loss tangent ($\tan \delta$) was calculated for the first time (to the best of our knowledge, not only in diamond but also for any point defect in insulators). The loss tangent is the ratio of the imaginary and real parts of the complex dielectric permittivity ϵ : $\tan \delta = \text{Im}(\epsilon)/\text{Re}(\epsilon)$ [42]. It is the imaginary part of the dielectric permittivity, associated with conductivity, which causes the absorption. The CRYSTAL code allows us to calculate the real and imaginary parts of the complex dielectric function $\epsilon(\nu)$ depending on the vibrational frequency ν (the maxima of the imaginary part of dielectric function correspond to frequencies of TO modes). The dependence of the loss tangent on the vibrational frequency is calculated in this case as the ratio of the imaginary and real parts of the obtained dielectric function.

The Figs. S8 and S9 in Supplementary present real and imaginary parts of dielectric function, respectively. Fig. 5a and b exhibit loss tangent function in normal and logarithmic scales, respectively.

As one can see, loss tangent for diamond with the *C-center* not exceed 0.1 for a whole range of vibrational frequencies, while its value does not

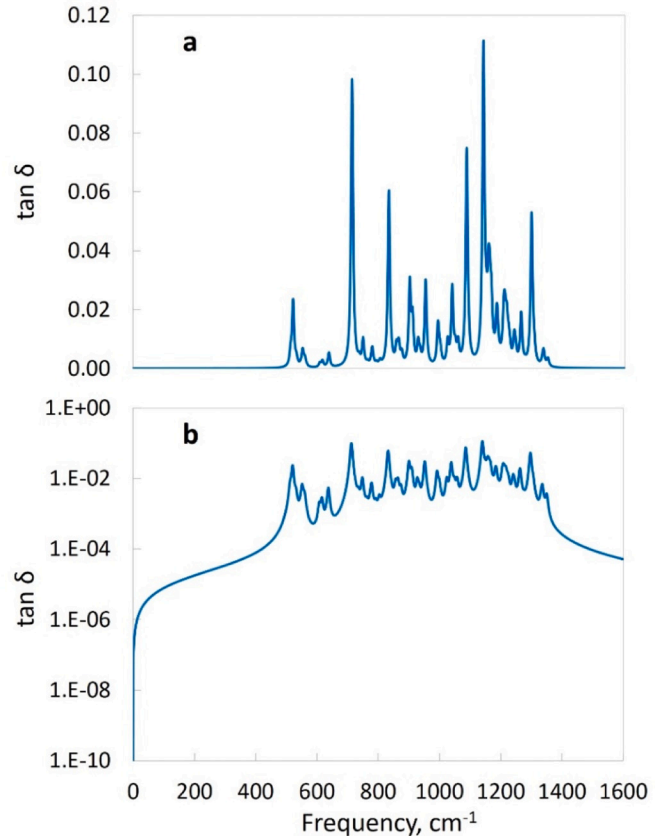


Fig. 5. Loss tangent ($\tan \delta = \text{Im}[\epsilon(\nu)]/\text{Re}[\epsilon(\nu)]$) for diamond with *C-center* in linear (a) and logarithmic (b) scales.

exceed 10^{-6} in the range 140–206 GHz used for plasma monitoring and electron cyclotron resonance (ECR) heating in fusion reactors (206 GHz correspond to 6.9 cm^{-1}). The main effect of N impurities is observed in the region $500\text{--}1400\text{ cm}^{-1}$, while beyond this range impurities practically do not affect dielectric material properties.

4. Conclusions

1) Nitrogen substitutional atoms (*C-centers*) form three chemical bonds with three nearest carbon atoms, which bond length is shorter than in pristine diamond, while the fourth nearest carbon atom has the most of unpaired spin and is displaced away from the nitrogen.

2) The *C-center* considerably affects the wide band gap of pristine diamond due to formation of two (occupied and unoccupied) defect energy bands. Note that the carbon atom with unpaired spin (but not nitrogen atom) gives the main contribution to the formation of these defect bands.

3) The *C-center* formation energy is $\sim 4\text{ eV}$.

4) Lattice constant of diamond with *C-center* slightly increases in comparison on the pristine diamond, while the elastic constants and moduli mostly decrease, that indicates less rigidity of the defective system (see Supplementary Section S2).

5) The Raman spectra, in general, may be used to identify single substitutional nitrogen atoms in the diamond. In diamond with the *C-center* the splitting of Raman peak is observed in narrow range $1300\text{--}1350\text{ cm}^{-1}$. We predict also N-induced optical absorption around 3 eV .

6) In general, the defect-induced features in IR spectra as well as in dielectric functions arise in the same phonon range of $400\text{--}1400\text{ cm}^{-1}$, definitely, at frequencies below the Raman peak in the pristine diamond.

7) The first *ab initio* calculations of the loss tangent for point defects in insulating materials were performed for the case of the N impurities in diamond. While loss tangent for diamond with the *C-center* can reach value 0.1 at some frequencies, its value does not exceed 10^{-6} in the frequency range important for fusion applications.

CRediT authorship contribution statement

L.L. Rusevich: Conceptualization, Methodology, Validation, Formal analysis, Investigation, Writing – original draft. **E.A. Kotomin:** Writing – review & editing, Validation. **A.I. Popov:** Resources, Writing – review & editing, Funding acquisition. **G. Aiello:** Writing – review & editing. **T. A. Scherer:** Writing – review & editing. **A. Lushchik:** Conceptualization, Methodology, Resources, Writing – review & editing, Supervision, Project administration, Funding acquisition.

Declaration of competing interest

The authors declare that they have no known competing financial interests or personal relationships that could have appeared to influence the work reported in this paper.

Data availability

Data will be made available on request.

Acknowledgments

Authors thank R. Dovesi, G. Zvejnicks and A. Platonenko for fruitful discussions. This study was supported by Eurofusion Enabling Research Project ENR-MAT.01.UT-T001-D001 “Investigation of defects and disorder in nonirradiated and irradiated Doped Diamond and Related Materials for fusion diagnostic applications (DDRDM) – Theoretical and Experimental analysis”. This work has been carried out within the framework of the EUROfusion Consortium, funded by the European Union via the Euratom Research and Training Programme (Grant

Agreement No 101052200 — EUROfusion). Views and opinions expressed are however those of the author(s) only and do not necessarily reflect those of the European Union or the European Commission. Neither the European Union nor the European Commission can be held responsible for them.

The research was performed in the Center of Excellence of the Institute of Solid State Physics, University of Latvia, supported through European Unions Horizon 2020 Framework Programme H2020-WIDESPREAD-01-2016-2017-TeamingPhase2 under grant agreement No. 739508, project CAMART².

Appendix A. Supplementary data

Supplementary data to this article can be found online at <https://doi.org/10.1016/j.diamond.2022.109399>.

References

- [1] R.B. Jackman, Special issue on diamond electronics, *Semic. Sci. Technol.* 18 (2003).
- [2] A. Mallik (Ed.), *Engineering Applications of Diamond*, Intech Open, 2021.
- [3] R.J. Narayan, R.D. Boehm, A.V. Sumant, Medical applications of diamond particles & surfaces, *Mater. Today* 14 (2011) 154–163, [https://doi.org/10.1016/S1369-7021\(11\)70087-6](https://doi.org/10.1016/S1369-7021(11)70087-6).
- [4] R. Schirhagi, K. Chang, M. Loretz, C.L. Degen, Nitrogen-vacancy centers in diamond: nanoscale sensors for physics and biology, *Annu. Rev. Phys. Chem.* 65 (2014) 83–105, <https://doi.org/10.1146/annurev-physchem-040513-103659>.
- [5] V. Parshin, B. Garin, S. Myasnikova, A. Orlenkov, in: *Proc. of the 10th Int. ITG-Conf. on Displays and Vacuum Electronics. Germany, 2004*, pp. 305–310.
- [6] V.V. Parshin, B.M. Garin, S.E. Myasnikova, A.V. Orlenkov, Dielectric losses in CVD diamonds in the millimeter-wave range at temperatures 300–900 K, *Radiophys. Quantum Electron.* 47 (2004) 974–981, <https://doi.org/10.1007/s11141-005-0039-0>.
- [7] H. Yamada, A. Meier, F. Mazzocchi, S. Schreck, T. Scherer, Dielectric properties of single crystalline diamond wafers with large area at microwave wavelengths, *Diam. Relat. Mater.* 58 (2015) 1–4, <https://doi.org/10.1016/j.diamond.2015.05.004>.
- [8] F. Mazzocchi, G. Aiello, A. Meier, S. Schreck, P. Spaeh, D. Strauss, T. Scherer, Diamond window diagnostics for nuclear fusion applications — early concepts, in: *EPJ Web of Conferences* 87, 2015, p. 04007, <https://doi.org/10.1051/epjconf/20158704007>.
- [9] F. Mazzocchi, S. Schreck, D. Strauss, G. Aiello, A. Meier, T. Scherer, Diamond windows diagnostics for fusion reactors — updates of the design, *Fusion Eng. Design* 123 (2017) 820–824, <https://doi.org/10.1016/j.fusengdes.2017.04.012>.
- [10] G.J. Schmid, J.A. Koch, R.A. Lerche, M.J. Moran, A neutron sensor based on single crystal CVD diamond, *Nucl. Instr. Meth. A* 527 (2004) 554–561, <https://doi.org/10.1016/j.nima.2004.03.199>.
- [11] S. Almagia, M. Marinelli, E. Milani, G. Prestopino, A. Tucciarone, C. Verona, G. Verona-Rinati, M. Angelone, D. Lattanzi, M. Pillon, R.M. Montecali, M. A. Vincenti, Thermal and fast neutron detection in chemical vapor deposition single-crystal diamond detectors, *J. Appl. Phys.* 103 (2008), 054501, <https://doi.org/10.1063/1.2838208>.
- [12] C. Manfredotti, CVD diamond detectors for nuclear and dosimetric applications, *Diam. Relat. Mater.* 14 (2005) 531–540, <https://doi.org/10.1016/j.diamond.2004.11.037>.
- [13] T. Shimaoka, S. Koizumi, J.H. Kaneko, Recent progress in diamond radiation detectors, *Funct. Diam.* 1 (2022) 205–220, <https://doi.org/10.1080/26941112.2021.2017758>.
- [14] Y. Tanimura, J. Kaneko, M. Katagiri, Y. Ikeda, T. Nishitani, H. Takeuchi, T. Iida, High-temperature operation of a radiation detector made of a type IIA diamond single crystal synthesized by a HP/HT method, *Nucl. Instrum. Methods Phys. Res. A* 443 (2000) 325–330, [https://doi.org/10.1016/S0168-9002\(99\)01048-7](https://doi.org/10.1016/S0168-9002(99)01048-7).
- [15] A. Crnjac, N. Skukan, G. Provatas, M. Rodriguez-Ramos, M. Pomorski, M. Jakšić, Electronic properties of a synthetic single-crystal diamond exposed to high temperature and high radiation, *Materials* 13 (2020) 2473, <https://doi.org/10.3390/ma13112473>.
- [16] M. Angelone, C. Verona, Properties of diamond-based neutron detectors operated in harsh environments, *J. Nucl. Eng.* 2 (2021) 422–470, <https://doi.org/10.3390/jne2040032>.
- [17] M. Tsubota, J.H. Kaneko, D. Miyazaki, T. Shimaoka, K. Ueno, T. Tadokoro, A. Chayahara, H. Watanabe, Y. Kato, S. Shikata, H. Kuwabara, High-temperature characteristics of charge collection efficiency using single CVD diamond detectors, *Nucl. Instrum. Methods A* 789 (2015) 50–56, <https://doi.org/10.1016/j.nima.2015.04.002>.
- [18] M. Passeri, F. Pompili, B. Esposito, M. Pillon, M. Angelone, D. Marocco, G. Pagano, S. Podda, M. Riva, Assessment of single crystal diamond detector radiation hardness to 14 MeV neutrons, *Nucl. Instrum. Methods A* 1010 (2021), 165574, <https://doi.org/10.1016/j.nima.2021.165574>.
- [19] L. Bani, A. Alexopoulos, M. Artuso, et al., A study of the radiation tolerance of CVD diamond to 70 MeV protons, fast neutrons and 200 MeV pions, *Sensors* 20 (2020) 6648, <https://doi.org/10.3390/s20226648>.

- [20] A.M. Zaitsev, *Optical Properties of Diamond: A Data Handbook*, Springer-Verlag, Berlin, 2001.
- [21] M.N.R. Ashfold, J.P. Goss, B.L. Green, P.W. May, M.E. Newton, C.V. Peaker, Nitrogen in diamond, *Chem. Rev.* 120 (2020) 5745–5794, <https://doi.org/10.1021/acs.chemrev.9b00518>.
- [22] C.M. Breeding, J.E. Shigley, *Gems Gemol.* 45 (2009) 96–111. Summer.
- [23] A. Zelferino, S. Salustro, J. Baima, V. Lacivita, R. Orlando, R. Dovesi, The electronic states of the neutral vacancy in diamond: a quantum mechanical approach, *Theor. Chem. Accounts* 135 (2016) 74, <https://doi.org/10.1007/s00214-016-1813-0>.
- [24] J. Prentice, B. Monserrat, R.J. Needs, First-principles study of the dynamic Jahn-Teller distortion of the neutral vacancy in diamond, *Phys. Rev. B* 95 (2017), 014108, <https://doi.org/10.1103/PhysRevB.95.014108>.
- [25] J. Baima, A. Zelferino, P. Olivero, A. Erba, R. Dovesi, Raman spectroscopic features of the neutral vacancy in diamond from ab initio quantum-mechanical calculations, *Phys. Chem. Chem. Phys.* 18 (2016) 1961–1968, <https://doi.org/10.1039/c5cp06672g>.
- [26] S. Vimolchalao, W.H. Liang, F.D. Vila, J. Kas, F. Farges, J. Rehr, Bethe-salpeter equation calculations of nitrogen-vacancy defects in diamond, *J. Phys. Chem. Sol.* 122 (2018) 87–93, <https://doi.org/10.1016/j.jpcs.2018.06.006>.
- [27] S. Salustro, A.M. Ferrari, F.S. Gentile, J.K. Desmarais, M. Rérat, R. Dovesi, Characterization of the B-center defect in diamond through the vibrational spectrum: a quantum-mechanical approach, *J. Phys. Chem. A* 122 (2018) 594–600, <https://doi.org/10.1021/acs.jpca.7b11551>.
- [28] E.B. Lombardi, A. Mainwood, K. Osuch, E.C. Reynhardt, Computational models of the single substitutional nitrogen atom in diamond, *J. Phys. Condens. Matter* 15 (2003) 3135–3149, <https://doi.org/10.1088/0953-8984/15/19/314>.
- [29] S. Salustro, G. Sansone, C.M. Zicovich-Wilson, Y. Noel, L. Maschio, R. Dovesi, The A-center defect in diamond: quantum mechanical characterization through the infrared spectrum, *Phys. Chem. Chem. Phys.* 19 (2017) 14478–14485, <https://doi.org/10.1039/c7cp00093f>.
- [30] S. Salustro, F. Pascale, W.C. Mackrodt, C. Ravoux, A. Erba, R. Dovesi, Interstitial nitrogen atoms in diamond. A quantum mechanical investigation of its electronic and vibrational properties, *Phys. Chem. Chem. Phys.* 20 (2018) 16615–16624, <https://doi.org/10.1039/c8cp02484g>.
- [31] A.M. Ferrari, S. Salustro, F.S. Gentile, W.C. Mackrodt, R. Dovesi, Substitutional nitrogen in diamond: a quantum mechanical investigation of the electronic and spectroscopic properties, *Carbon* 134 (2018) 354–365, <https://doi.org/10.1016/j.carbon.2018.03.091>.
- [32] T. Nishimura, T. Katayama, S. Mo, A. Chikamatsu, T. Hasegawa, Improvement of electric insulation in dielectric layered perovskite nickelate films via fluorination, *J. Mater. Chem. C* (2022), <https://doi.org/10.1039/d1tc04755h>.
- [33] R. Dovesi, V.R. Saunders, C. Roetti, R. Orlando, C.M. Zicovich-Wilson, F. Pascale, B. Civalieri, K. Doll, N.M. Harrison, I.J. Bush, P. D'Arco, M. Llunell, M. Causà, Y. Noel, L. Maschio, A. Erba, M. Rerat, S. Casassa, *CRYSTAL17 User's Manual*, University of Torino, Torino, 2017.
- [34] G.J.B. Hurst, M. Dupuis, E. Clementi, Ab initio analytic polarizability, first and second hyperpolarizabilities of large conjugated organic molecules: applications to polyenes C₄H₆ to C₂₂H₂₄, *J. Chem. Phys.* 89 (1988) 385–395, <https://doi.org/10.1063/1.455480>.
- [35] B. Kirtman, F.L. Gu, D.M. Bishop, Extension of the genkin and mednis treatment for dynamic polarizabilities and hyperpolarizabilities of infinite periodic systems. I. Coupled perturbed Hartree-Fock theory, *J. Chem. Phys.* 113 (2000) 1294–1309, <https://doi.org/10.1063/1.481907>.
- [36] R. Dovesi, B. Kirtman, L. Maschio, J. Maul, F. Pascale, M. Rérat, Calculation of the infrared intensity of crystalline systems. A comparison of three strategies based on Berry phase, Wannier function, and coupled-perturbed Kohn-Sham methods, *J. Phys. Chem. C* 123 (2019) 8336–8346, <https://doi.org/10.1021/acs.jpcc.8b08902>.
- [37] L.L. Rusevich, E.A. Kotomin, G. Zvejnieks, A.I. Popov, Ab initio calculations of structural, electronic and vibrational properties of BaTiO₃ and SrTiO₃ perovskite crystals with oxygen vacancies, *Low Temp. Phys.* 46 (2020) 1185–1195, <https://doi.org/10.1063/1.51002472>.
- [38] L. Maschio, B. Kirtman, M. Rérat, R. Orlando, R. Dovesi, Ab initio analytical raman intensities for periodic systems through a coupled perturbed Hartree-Fock/Kohn-Sham method in an atomic orbital basis. I. Theory, *J. Chem. Phys.* 139 (2013), 164101, <https://doi.org/10.1063/1.4824442>.
- [39] L. Maschio, B. Kirtman, M. Rérat, R. Orlando, R. Dovesi, Ab initio analytical raman intensities for periodic systems through a coupled perturbed hartree-Fock/Kohn-Sham method in an atomic orbital basis. II. Validation and comparison with experiments, *J. Chem. Phys.* 139 (2013), 164102, <https://doi.org/10.1063/1.4824443>.
- [40] P.R. Briddon, R. Jones, Theory of impurities in diamond, *Physica B* 185 (1993) 179–189, [https://doi.org/10.1016/0921-4526\(93\)90235-x](https://doi.org/10.1016/0921-4526(93)90235-x).
- [41] L.L. Rusevich, M. Tyunina, E.A. Kotomin, N. Nepomniashchaia, A. Dejneka, The electronic properties of SrTiO_{3-δ} with oxygen vacancies or substitutions, *Sci. Rep.* 11 (2021) 23341, <https://doi.org/10.1038/s41598-021-02751-9>.
- [42] J. Baker-Jarvis, S. Kim, The interaction of radio-frequency fields with dielectric materials at macroscopic to mesoscopic scales, *J. Res. Natl. Ins. Standards Technol.* 117 (2012) 1–60, <https://doi.org/10.6028/jres.117.001>.